Comparative modelling of laboratory experiments for the hydro-mechanical behaviour of a compacted bentonite–sand mixture

Comparative modelling of laboratory experiments for the hydro-mechanical behaviour of a compacted bentonite-sand mixture

A. Millard[1*], N. Mokni[2], J.D. Barnichon[2], K.E. Thatcher[3], A.E. Bond[3], A. Fraser-Harris[4], C. Mc Dermott[4], R. Blaheta[5], Z. Michalec[5], M. Hasal[5], T.S. Nguyen[6], O.Nasir[7], R. Fedors[8], H. Yi[9], O. Kolditz[9]

[1] *Commissariat à l'énergie atomique et aux énergies alternatives, France*

[2] *Institut de Radioprotectioçn et de Sureté Nucléaire, France*

[3] *Quintessa, UK*

[4] *University of Edinburgh, UK*

[5] *Institue of Geonic CAS, Czech Republic*

[6] *Canadian Nuclear Safety Commission, Canada*

[7] *Geofirma, Canada*

[8] *Nuclear Regulatory Commission, USA*

[9] *UFZ, Germany*

Abstract: A comparative modelling exercise involving several independent teams from the DECOVALEX-2015 project is presented in this paper. The exercise is based on various laboratory experiments that have been carried out in the framework of a French research program called SEALEX and conducted by the IRSN. The program focuses on the long-term performance of swelling clay-based sealing systems that provide an important contribution to the safety of underground nuclear waste disposal facilities. A number of materials are being considered in the sealing systems; the current work focuses on a 70/30 MX80 bentonite-sand mixture compacted at dry densities between 1.67 Mg/m^3 and 1.97 Mg/m^3. The improved understanding of the full set of hydro-mechanical processes affecting the behaviour of an in-situ sealing system requires both experiments ranging from small-scale laboratory tests to full-scale field emplacement studies, and coupled hydro-mechanical models that are able to explain the observations in the experiments. The approach was to build models of increasing complexity starting for the simplest laboratory experiments and building towards the full-scale in situ experiments. Following this approach, two sets of small-scale laboratory experiments have been performed and modelled. The first set of experiments involve characterising the hydro-mechanical behaviour of the bentonite-sand mixture by means of (i) water retention tests under both constant volume and free swell conditions, (ii) infiltration test under constant volume condition, and (iii) swelling and compression tests under suction control conditions. The second, more complex, experiment is a 1/10th scale mock-up of a larger scale in situ experiment. Modelling of the full-scale experiment is described in a companion paper. A number of independent teams have worked towards modelling these experiments using different conceptual models, codes, and input parameters. Their results are compared and discussed. This exercise has enabled an improved modelling of the bentonite-sand mixture behaviour, in particular accounting for the dependence of its retention curve on the dry density. Moreover, it has shown the importance of the technological voids on the short-term behaviour of the sealing system.

.

Key words: hydro-mechanical (HM) coupling; numerical modelling; sealing systems; compacted bentonite-sand mixture.

1 Introduction

After the construction and operation phases of a radioactive waste repository, the repository closing procedure will involve installing sealing systems in order to ensure the long-term containment function of the repository. These systems, which act as hydraulic plugs, should minimize the water flow along the boreholes, the galleries and the access shafts, limiting and delaying the migration of radionuclides to the biosphere. Sealing of boreholes is common in the oil and gas industry, where mechanical and cement-related devices are often used. For radioactive waste

Doi:

*Corresponding Author.E-mail:alain.millard@cea.fr

repositories, the sealing systems often consist of a swelling core, confined by some rigid blocks at both ends (Hansen et al., 2013). The swelling core is mainly made of bentonite, which has not only a very low hydraulic conductivity and a high sorption capability, but also a strong swelling potential, capable of clogging all the voids. Moreover, when confined, it can develop a swelling pressure which can partially close the fractures in the host rock generated by the excavation. The feasibility of such sealing devices has been demonstrated by means of in situ experiments performed in Underground Research Laboratories (URL), such as TSX (Tunnel Sealing Experiment) (Martino et al., 2008) and ESP (Enhanced Sealing Project) (Dixon et al., 2014) at Atomic Energy of Canada Limited (AECL)'s URL in Canada, FEBEX (Full-scale Engineered Barriers Experiment) at Grimsel, Switzerland (Huertas et al., 2000), EB (Engineered Barrier Emplacement Experiment) at the Mont Terri, Switzerland (Villar et al., 2014), RESEAL (Repository Sealing) at Hades URL, Belgium (van Geet et al., 2007) and KEY at the Laboratoire souterrain de Meuse Haute Marne (LSMHM), France (Barnichon and Deleruyelle, 2009). In addition, the French Institut de Radioprotection et de Sureté Nucléaire (IRSN) has conducted the SEALEX (Sealing Performace Experiment) project in the Tournemire URL, in order to test various technical parameters that could influence the global hydraulic and mechanical performance of a seal, and to provide the IRSN with feedback and knowledge on the key parameters (Barnichon and Deleruyelle, 2009).

The in situ experiments in the SEALEX project involve a series of sealing systems emplaced in large diameter (60 cm) horizontal boreholes excavated in argillite. Dimensions of the clay core have been defined by scoping calculations on saturation kinetics (Barnichon et *al*., 2012). These were defined to be as representative as possible of the French concept and taking into account the re-saturation time in order to perform tests in a reasonable schedule (Barnichon et *al*., 2012). An annular void space is required for emplacement of the core. The confinement system is fitted to prevent the core swelling in the axial direction. Water for resaturation of the core is supplied from a tank in the experimental gallery under a controlled pressure head. Hydration has been performed following 2 phases: First, a back pressure of 0.2 MPa was applied in the tank, which allowed filling the gap between the rock and the device in 2 hours. Second, the back pressure was removed, and the upper level of the water in the tank was constantly maintained at 1m above the axis of the borehole (i.e. 1m water head). The core material in the sealing system is a 70/30 mixture of MX80 bentonite-sand compacted at different dry densities ranging from 1.65 to 1.97 Mg/m^3 and chosen so as to target a 4 MPa maximum swelling pressure; the potential swelling pressure is strongly correlated to the initial dry density (other influencing factors such as pore water salinity are out of the scope of this study) of the montmorillonite fraction (80%), which is the main mineralogical component of MX80 bentonite. Before modelling the full-scale in situ tests, which are described in a companion paper (Millard et al., 2016), several laboratory tests were utilized as the first steps in the modelling exercise to characterize the hydro-mechanical properties of the 70/30 mixture of MX80 bentonite-sand.

Several laboratory experiments of increasing complexity have been carried out to finalize the specifications as well as the characterization of this material, and also to provide input data required for modelling of the SEALEX full-scale in situ test. The set of laboratory experiments to characterise the hydro-mechanical behaviour of the bentonite-sand mixture included (i) water retention tests performed under both constant volume and free swell conditions, (ii) infiltration test performed under constant volume condition, and (iii) swelling and compression tests performed under suction control conditions. A more complex experiment, a $1/10^{th}$ scale mock-up, was carried out to represent the full-scale experiments but without the interactions with the argillite. A monolithic cylindrical sample was hydrated in a rigid stainless steel cell. Synthetic water was first injected at the bottom of the sample, while maintaining an axial confinement. A confinement loss phase followed, that consisted in of removing the axial confining pressure to mimic the long-term failure of confinement blocks in real repositories that is considered in some disruptive scenarios for a typical repository. Finally, a new confinement phase was performed after reaching a 20% axial strain at the end of the confinement loss phase.

The key features and processes that should be captured in the modelling of these experiments are:

(1) Resaturation of a pre-compacted clay-based core under free and confined conditions, leading to complex load/suction paths;

(2) Development of a high swelling pressure;

(3) Continuous evolution of the dry density of the material, with significant impact on the hydro-mechanical properties;

(4) Influence of the voids surrounding the core.

This collaborative modelling exercise was coordinated under the DECOVALEX (DEvelopment of COupled models and their VALidation against EXperiments) project. DECOVALEX was set up to support the development of computer codes in the framework of radioactive wastes disposal, and to compare model calculations with results from field and laboratory experiments. More information on the DECOVALEX project may be found at www.decovalex.org. In the latest phase of the project (2012–2015), referred to as DECOVALEX-2015, the SEALEX project was one of the tasks identified for a modelling exercise. This particular DECOVALEX task was split into four steps:

(1) The identification of relevant processes and calibration of bentonite-sand mixture parameters on the basis of laboratory tests (water retention curves, infiltration test under constant volume condition, swelling and compression tests under suction control condition),

(2) The modelling of a 1/10th scale mock-up representative of the in-situ SEALEX experiments,

(3) The modelling of hydraulic behaviour of the rock surrounding the bentonite-sand plug, based on the in-situ WT-1 test results,

(4) The modelling of the hydro-mechanical behaviour of the bentonite-sand plug, based on the in-situ PT-A1 test results.

The results from the first two steps are described in this paper; the two other steps are treated in a companion paper (Millard et al., 2016).

The teams that participated in this modelling exercise and their corresponding funding organisations are:

(1) CNSC (Canadian Nuclear Safety Commission, Canada)

(2) IRSN (Institut de Radioprotection et de Sûreté Nucléaire, France);

(3) Quintessa on behalf of RWM (Radioactive Waste Management, Ltd., UK);

(4) UoE (University of Edinburgh) on behalf of RWM (Radioactive Waste Management, Ltd., UK);

(5) UGN (Institute of Geonics CAS) on behalf of RAWRA (RadioActive Waste Repository Authority, Czech Republic);

(6) NRC (Nuclear Regulatory Commission, USA);

(7) UFZ (Helmholtz Centre for Environmental Research, Germany).

2 Theoretical formulations

Formulations used by the teams consider the following aspects of the experiments. All the tests considered in the task were isothermal (temperature close to constant), thus thermal or thermally coupled processes could be discarded. Therefore, hydro-mechanical processes in unsaturated and saturated regimes could be expected to prevail in these experiments. However, physiochemical effects could not be ruled out a priori, especially in the large macro-voids where the bentonite-sand core could, after flooding, initially exfoliate at its outer boundaries thus creating a bentonite-based gel (as observed in specifically designed experiments, Saba 2014). Irrespective of this potential physiochemical process, with the progressive saturation and swelling of the core, this gel likely would be progressively re-compacted.

In the following summary, the common aspects of the formulations used by the teams are described and the different aspects of each team's formulation are highlighted.

2.1 Common basis

Hydro-mechanical processes taking place in the bentonite-sand core can be described by applying the classical framework of multi-phase flow in deformable porous media. The general formulation of multi-phase flow includes liquid water, vapor and dry air (Olivella et al., 1994, 1996). The total mass of water per unit volume of the porous medium under unsaturated conditions is $\rho_w \vartheta S_w + \rho_g \vartheta S_g$, where ρ_w is the liquid phase density, ρ_g is the gas phase density, ϑ the porosity and S_w and S_g are respectively the degree of saturation (volumetric fraction) of liquid and gas in the pores. The total water mass balance is expressed as:

$$\frac{\partial}{\partial t}\left(\rho_w \vartheta S_w + \rho_g \vartheta S_g\right) + div(\boldsymbol{j_w} + \boldsymbol{j_v}) = 0 \qquad (1)$$

where $\underline{\boldsymbol{j_w}}$ and $\underline{\boldsymbol{j_v}}$ are respectively the total fluxes of liquid water and water vapour.

Neglecting the generally small influence of air dissolved in liquid water, the total mass of dry air per unit volume of the porous medium is $\rho_a \vartheta S_g$ where ρ_a is the dry air density. The total dry air mass balance is expressed as:

$$\frac{\partial}{\partial t}\left(\rho_a \vartheta S_g\right) + div(\boldsymbol{j_a}) = 0 \qquad (2)$$

where $\underline{\boldsymbol{j_a}}$ is the total flux of dry air.

Finally the momentum balance of the whole porous medium reduces to the equilibrium of stresses if inertial terms are neglected:

$$div\, \boldsymbol{\sigma} + \boldsymbol{b} = 0 \qquad (3)$$

where $\boldsymbol{\sigma}$ is the total stress tensor and $\boldsymbol{b}$ is the vector of body forces.

The flow of water is expressed in terms of the average velocity of the liquid phase $\boldsymbol{q_l}$ as $\boldsymbol{j_w} = \rho_w \boldsymbol{q_l}$ whereas the flow of vapour is the sum of advective and diffusive terms:

$$\boldsymbol{j_v} = \rho_v \boldsymbol{q_g} + \boldsymbol{i_v} \qquad (5)$$

where $\boldsymbol{q_g}$ is the average velocity of the gas phase, ρ_v is the vapour density and $\boldsymbol{i_v}$ is the diffusive flux of vapour in the gas. The flow of dry air has a similar decomposition:

$$\boldsymbol{j_a} = \rho_a \boldsymbol{q_g} + \boldsymbol{i_a} \qquad (6)$$

where $\boldsymbol{i_a}$is the diffusive flux of dry air in the gas. The flows $\boldsymbol{q_l}$ and $\boldsymbol{q_g}$ are given by generalized Darcy's laws:

$$\boldsymbol{q_l} = -\frac{\boldsymbol{K} k_{rl}}{\mu_l} \boldsymbol{\nabla} p_l \qquad (7)$$

$$\boldsymbol{q_g} = -\frac{\boldsymbol{K} k_{rg}}{\mu_g} \boldsymbol{\nabla} p_g \qquad (8)$$

where p_i is the partial pressure of liquid water (i=l) and gas (i=g) respectively, $\boldsymbol{K}$ is the intrinsic permeability, k_{ri} the relative permeabilities (depending on liquid saturation) and μ_i the dynamic viscosities.
Vapour diffusion is expressed by Fick's law:

$$\boldsymbol{i_v} = -\vartheta \rho_g S_g \boldsymbol{D} \boldsymbol{\nabla} \omega_v = -\boldsymbol{i_a} \qquad (9)$$

where $\boldsymbol{D}$ is the vapour diffusion coefficient and ω_v is the mass fraction of vapour.
In the present case of isothermal evolutions, the above equations can be simplified assuming that the gas pressure remains at atmospheric pressure, and neglecting the mass of vapour in front of the mass of liquid water. This leads to the well-known Richards' equation (Richards, 1931):

$$\frac{\partial}{\partial t}(\rho_w \vartheta S_w) + div(\boldsymbol{j_w} + \boldsymbol{j_v}) = 0 \qquad (10)$$

which includes a diffusive vapour flux that can be significant for low permeability clay-based materials. This approximation was found to be valid for the present modelling exercise and was used by CNSC, Quintessa, UGN, UoE, and UFZ, whereas IRSN used the complete formulation.

Most of the teams chose to describe the mechanical behaviour of the skeleton by a relationship between the effective stresses $\boldsymbol{\sigma}'$ calculated as:

$$\boldsymbol{\sigma}' = \boldsymbol{\sigma} + \chi \bar{p}\, \boldsymbol{I}$$

where χ is a hydro-mechanical coupling coefficient generally depending on the degree of saturation S_w and $\bar{p}$ is an effective pore pressure, and the strain $\boldsymbol{\varepsilon}$, which is partitioned into an elasto-plastic component $\boldsymbol{\varepsilon}^{ep}$ (sometimes reduced to a pure elastic component $\boldsymbol{\varepsilon}^{e}$) and a swelling component $\boldsymbol{\varepsilon}^{sw}$:

$$d\boldsymbol{\varepsilon} = d\boldsymbol{\varepsilon}^{ep} + d\boldsymbol{\varepsilon}^{sw}$$

Differences between the theoretical formulations used by the teams came essentially from the hydro-mechanical constitutive equations of the bentonite-sand mixture. They are compared in the next paragraph.

The different codes used by the Teams are listed in given in Table 1. Most of the codes are finite element codes and only QPAC, the code used by Quintessa, is based on finite volumes for hydraulics and mixed elements for mechanics (Maul, 2013).

Table 1. Computer codes and models

Team	Codes	Reference	Numerical method	Flow modelling
CNSC	COMSOL	COMSOL, 2012	Finite elements	Richards
IRSN	CODE_BRIGHT	Olivella et al.,1994, 1996	Finite elements	Two phase flow
Quintessa	QPAC	Quintessa, 2013	Finite volumes and mixed elements	Richards
UGN	COMSOL	COMSOL, 2012	Finite elements	Richards
NRC	FLAC3D	Itasca Consulting Group, 2011	Finite differences	NA
UoE	OGS	Kolditz et al., 2012	Finite elements	Richards
UFZ	OGS	Kolditz et al., 2012	Finite elements	Richards

2.2 Hydraulic constitutive equations

Water retention curve

The relationship between the suction (s) defined by $s = p_g - p_l$, and the liquid degree of saturation (S_w) is a key ingredient in the description of unsaturated porous media. It is often idealised by the van Genuchten retention curve:

$$S_e = \left[1 + \left(\frac{s}{P_0}\right)^{\frac{1}{1-\lambda_0}}\right]^{-\lambda_0} \qquad (11)$$

where the effective saturation S_e is defined by:

$$S_e = \frac{S_w - S_r}{S_s - S_r} \qquad (12)$$

S_r is the residual saturation, S_s is the saturation degree in saturated conditions, and P_0 and λ_0 are material parameters that can be identified from an experimental water retention curve. For pure bentonite, such curves correlate with the dry density of the material (Man and Martino, 2009). Because the dry density property is not a constant for bentonites as water content or mechanical stress evolve, the modelling teams needed to consider how the water retention curve had to be modified to account for the potential changes of dry density of the bentonite-sand mixture during the tests.

CNSC used the following equation to relate effective saturation and pressure head (h):

$$S_e = [1 + (\alpha_{EMDD} h)^N]^{-m} \quad (13)$$

where N and m are fitting parameters and α_{EMDD} is a coefficient that depends on the effective Montmorillonite dry density EMDD of the bentonite-sand mixture defined by:

$$EMDD = \frac{f_m . f_c . \rho_d}{\left[1 - \left(\frac{(1 - f_c)\rho_d}{G_a . \rho_w}\right) - \left(\frac{(1 - f_m) f_c . \rho_d}{G_n . \rho_w}\right)\right]} \quad (14)$$

$$\alpha_{EMDD} = \left(0.0705 \times (EMDD)^2 - 0.3065 \times (EMDD) + 0.313\right) \times F_{Corr} \quad (15)$$

In the above equation, f_m is the mass fraction of montmorillonite in clay fraction, f_c the mass fraction of clay in dry solid, ρ_d the dry bulk density, ρ_w the water density, G_a the relative density of aggregate component (specific gravity), G_n the relative density of non-montmorillonite clay component and F_{corr} a calibration parameter. The EMDD concept works well for estimations of the swelling pressure, hydraulic conductivity and the characteristics of the water retention curve under saturated and unsaturated conditions based on regression studies by Baumgartner (2006).

IRSN used the van Genuchten relation (Eqn. 11) but chose to let the parameters P_0 and λ_0 depend on porosity variation $\vartheta_0 - \vartheta$, where ϑ_0 is the initial porosity, such that:

$$P_0 = \bar{P}_0 e^{a(\vartheta_0 - \vartheta)} \qquad \lambda_0 = \bar{\lambda}_0 e^{b(\vartheta_0 - \vartheta)} \quad (16)$$

To reflect the influence of the double structure porosity of the bentonite, as accounted for in the BExM model (Navarro et al., 2015), Quintessa, used a water retention curve relating the suction under free swelling conditions s_{free} to the water content by mass ω, and the dry density:

$$s_{free} = \alpha \exp(\beta \rho_d) + \gamma \exp(\varepsilon \omega)) \quad (17)$$

where $\alpha, \beta, \gamma, \varepsilon$ are constants calibrated against the laboratory tests results. The suction is explicitly linked to the mean total stress p through the following equation, suggested by Dueck (2004):

$$s = s_{free} - p \quad (18)$$

For UoE, water retention curve is fitted with an empirical relationship derived by Bond and Benbow (2009), giving also the free suction:

$$s_{free} = M_b\big(exp(a - b\omega) + exp(c - d\omega)\big) \quad (19)$$

where M_b is the mass fraction of bentonite, and *a, b, c,* and *d* are constants calibrated against the laboratory tests results.

As Quintessa, UGN used a relation between the water content (ω), the suction and the dry density:

$$\omega = \begin{cases} \omega(s) = a \cdot \ln(s) + b & for\ \omega(s) < \omega_{max} \\ \omega_{max} & elsewhere \end{cases} \quad (20)$$

This relation is constructed for a given dry density, by considering a simple bilinear representation of the experimental data in the ln(s) -ω plane. The relation (20) changes in time with the evolution of saturation and swelling strain, which changes the dry density and consequently enters the relation (20) through ω_{max} ,

$$\omega_{max} = \frac{\rho_s - \rho_d}{\rho_s}\frac{\rho_w}{\rho_d} + \omega_{res} \quad (21)$$

where ρ_s is the density of solid. The value ω_{res} could be related to the dry density of the bentonite component, but it was found that for the performed modelling it is sufficient to keep a constant value of ω_{res} (derived from the data provided for the bentonite sand mixture with dry density $1.67 Mg/m^3$). The effective water saturation is obtained from the water content through:

$$S_e = \frac{\omega - \omega_{res}}{\omega_{max} - \omega_{res}} \quad (22)$$

Finally, NRC and UFZ used the basic van Genuchten expression (10) without modification.

Permeability

The liquid water relative permeability was taken by all teams as a power law of the effective saturation degree:

$$k_{rl} = A\, S_e^{\beta} \quad (23)$$

Because of the changes of porosity in the material, some modifications of the intrinsic permeability were implemented. IRSN, CNSC and UGN let the intrinsic permeability follow the Kozeny-Carman's model:

$$K = K_0 \frac{\vartheta^3}{(1-\vartheta)^2}\frac{(1-\vartheta_0)^2}{\vartheta_0^3} \quad (24)$$

For Quintessa, the intrinsic permeability evolved with dry density according to:

$$K = K_0 10^{DD(\rho_d)} \quad (25)$$

wherethe empirical function $DD(\rho_d)$ was calibrated to test data (Thatcher et al, 2016).

For UoE, the intrinsic permeability variation was adapted for a bentonite-sand mixture from the Kozeny-Carman relationship after the method of Liu et al. (2011) by a scaled pore-shape factor (C_k) that reflects the observation that the Kozeny constant increases with increasing volume fraction of bentonite. This is further adjusted to account for the mass fraction of montmorillonite within the solid grains ϑ_p :

$$K = \frac{\delta_p^2}{4 C_k \vartheta_p^2}\frac{\vartheta^m}{(1-\vartheta)^n} \quad (26)$$

where C_k is a constant and δ_p is the average montmorillonite sheet thickness, and m, n are constants calibrated against the laboratory tests results.

UFZ used constant intrinsic permeability, with different values according to the initial dry density of the material.

2.3 Mechanical constitutive equations

Effective stresses

CNSC and UGN used an effective stresses $\boldsymbol{\sigma}'$ calculated as:

$$\boldsymbol{\sigma}' = \boldsymbol{\sigma} + b\bar{p}\,\boldsymbol{I} \qquad (27)$$

where b stands for the classical Biot's coefficient and the effective pore pressure $\bar{p}$ is defined by:

$$\bar{p} = \max(p_w, p_g) \qquad (28)$$

NRC invoked the Bishop generalized principle of effective stress (Fredlund and Rahardjo, 1993) according to:

$$\boldsymbol{\sigma}' = \boldsymbol{\sigma} + (p_a - \chi s)\,\boldsymbol{I} \qquad (29)$$

where p_a is the air pressure, and χ the Bishop's parameter, which is a function of the effective saturation S_e :

$$\chi = S_e \qquad (30)$$

Different relationships between the Bishop parameter and the effective saturation were explored. However, the simplest relationship, as shown in equation 30, was found to be sufficient for calibrations of the experimental data described in this paper.

For UoE, only a fraction of the free suction was converted to a stress change, through an empirically calibrated internal strain factor β_ε used as a replacement to the classical Biot's constant:

$$\boldsymbol{\sigma}' = \boldsymbol{\sigma} - \beta_\varepsilon S_w\, s_{free}\boldsymbol{I} \qquad (31)$$

Finally for UFZ, the effective stresses were simply defined as:

$$\boldsymbol{\sigma}' = \boldsymbol{\sigma} - S_w p_w \boldsymbol{I} \qquad (32)$$

Elastoplastic behaviour

IRSN used the well-known mechanical elasto-plastic Barcelona Basic Model (Alonso et al., 1990), with variable volumetric elastic properties with respect to mean net stress p, defined as the excess of total stress over gas pressure, and suction s:

$$d\varepsilon_v^e = \frac{\kappa_i(s)}{1+e}\frac{dp}{p} + \frac{\kappa_s(p)}{1+e}\frac{ds}{s+0.1} \qquad (33)$$

In this expression, κ_i and κ_s are elastic stiffness parameters for changes in net mean stress and suction respectively. The elastic stiffness parameter for changes in net mean stress depends on suction as:

$$\kappa_i(s) = \kappa_{i0}(1 + \alpha_i s) \qquad (34)$$

where κ_{i0} is the elastic stiffness parameter in saturated conditions and α_i a model parameter. The elastic stiffness parameter for suction changes depends in turn on mean stress as:

$$\kappa_s(p) = \kappa_{s0}\left(1 + \alpha_s ln\frac{p}{p_{ref}}\right) \qquad (35)$$

where κ_{s0}, α_s and p_{ref} are model parameters.

For NRC, the elasto-plastic behaviour was described by the classical Modified Cam-Clay model using the slope of the virgin consolidation curve λ_s, the slope of the recompression (unloading) curve κ, the reference specific volume v_{ref0} for the recompression curve at a reference state p_{ref}, and the initial preconsolidation pressure p_{c0}. The reference specific volume is treated as a function of suction using the relation:

$$v_{ref0} = v_{max} - \frac{s}{v_a + v_b\, s} \qquad (36)$$

where v_{max}, v_a, and v_b are empirical curve fitting parameters estimated from oedometer compression data in Wang et al. (2013a).

The bulk modulus K is treated as a function of the mean effective stress according to:

$$K = \frac{1}{\kappa_r}\left[\omega_0 + \frac{\omega-\omega_0}{1+b(\omega-\omega_0)}\right] \quad (37)$$

where ω is the product of the specific volume v and the mean effective stress p, and the parameter b is given by:

$$b = \frac{1}{\kappa_r K_\infty - \omega_0} \quad (38)$$

where K_∞ is the maximum bulk modulus.

The Quintessa mechanical model was based on the Modified Cam Clay (MCC) model, with some small modifications. The elastic bulk modulus is given by:

$$K = K_0 - \kappa\, p' \quad (39)$$

and the plastic yield surface is given by:

$$\left[\frac{q}{M}\right]^2 + p'\,(p' - p_c) = 0 \quad (40)$$

where K is the bulk modulus, p' is effective mean stress, q is deviatoric stress, p_c is the pre-consolidation pressure and K_0, v_κ, κ, M are all constant parameters. The virgin consolidation line is based on an original relationship, called ILC (Internal Limit Curve, Thatcher et al., 2016) that is based on relationships derived from published data (Wang et al., 2012) and on a conceptual understanding of energy balances in the bentonite. It is used to parametrize both the water retention curve and the plastic failure of the material. It relates the effective mean stress (or swelling pressure) to the dry density (or water content):

$$p = \alpha * exp(\beta \rho_d) \quad (41)$$

UoE used a non-linear elastic strain dependent model, where the elastic modulus is updated as a function of the total volumetric strain:

$$E_t = E_0(1 - (\alpha \sum_{t=1}^{t-1} \varepsilon_v)^d) \quad (42)$$

where E_0 is the reference starting Young's Modulus, α is the hardening or softening factor depending on the strain direction, ε_v is the total volumetric strain, and d is a fitting parameter. This function leads to an increase in elastic modulus with a decrease in sample volume i.e. consolidation hardening, and vice-versa. The initial void ratio of the sample is used as a control to switch between the softening and hardening factors in the calculation of the Young's modulus. This allows softening and hardening parameters that reflect the different stress states and strain directions to be defined separately.

To account for the compressive strains associated with the plastic collapse experimentally observed in the mock-up test, a stress dependent source term is applied. A mean vertical stress ($\bar{\sigma}_z$) threshold is defined by the relationship between suction and pre-consolidation pressure in the consolidation tests (Wang et al., 2013b). The applied source term is scaled by the volume of the sample that has a stress in excess of this threshold via a calibrated curve:

$$\sigma_{ST} = f(\bar{\sigma}_z) = \begin{cases} ST, & \bar{\sigma}_z < threshold \\ 0, & \bar{\sigma}_z \geq threshold \end{cases} \quad (43)$$

UGN used an incremental elasticity model with a constant Poisson's ratio and a variable elasticity modulus, function of dry density:

$$E = \xi \exp\left(\alpha \frac{\rho_d}{\rho_w}\right) \quad (44)$$

ξ and α being material parameters.

Finally, UFZ and CNSC chose an isotropic linear elastic model, with constant parameters.

However, in order to be able to model the laboratory compression tests under suction control, which exhibited a permanent strain response upon unloading, UGN and UFZ also used the modified Cam-Clay for the simulation of these particular tests.

Swelling strain

Except for IRSN and UoE, all the teams had to incorporate an additional swelling strain to be able to reproduce the swelling behaviour of the bentonite-sand mixture. For CNSC, the swelling strain increment was proportional to the suction increment *ds*, through a constant coefficient:

$$d\boldsymbol{\varepsilon}^{sw} = B_s\, ds\, \boldsymbol{I} \quad (45)$$

Whereas, for NRC, the swelling strain increment was calculated using the unit swelling parameter α_{cw} as follows:

$$\mathrm{d}\boldsymbol{\varepsilon}^{sw} = \frac{1}{3}\,\alpha_{cw}\,\mathrm{d}\omega\,\boldsymbol{I} \quad (46)$$

where dω is the water content increment. The unit swelling parameter represents the slope of the relationship between strain and water content. The experimental data from Wang et al. (2013b) was used to estimate the value of the unit swelling parameter for the bentonite-sand mixture. The fit for α_{cw} used equations for two different parts of the water content range as follows:

$$\alpha_{cw} = \frac{a - c\,\omega^2}{(a + b\omega + c\omega^2)^2} \quad for\ 0 \le \omega \le 0.129 \quad (47)$$

$$\alpha_{cw} = 0.134 \quad for\ 0.129 \le \omega \le 0.254 \quad (48)$$

where a=100, b=-326.24, and c=-2.85e3. The first equation for α_{cw} forces the unit swelling to zero as water content approaches zero and covers the range where no measurements were provided. The unit swelling values from the above equations were derived assuming a constant dry bulk density, and were only used for modeling of the free swelling and compression oedometer tests in section 3.2

Quintessa accounted for the swelling of the bentonite through an additional strain source term in the mechanical constitutive equations, based on the amount of water calculated in a computational compartment (according to the finite volume approximation used). This swelling strain was calculated in the three principal directions, assuming that bentonite clay sheets are oriented randomly such that one third of the clay sheets can be associated with each of the principal directions, as follows:

$$\varepsilon_{nn}^{sw} = \frac{a}{3}\,\frac{(\omega_{nn} - \omega_0)m_s}{\rho_w V_{comp}} \quad (49)$$

where ω_0 is the initial water content, ω_{nn} is the water content in direction n, m_s is the mass of solids, V_{comp} is the compartmental volume and a is a swelling efficiency term that reflects that not all additional water will cause a volume increase, some will just fill void space in the sample.

UGN also chose to express the swelling strain as a function of change in water mass content:

$$\boldsymbol{\varepsilon}^{sw} = \gamma\frac{\rho_d}{\rho_w}(\omega - \omega_{init})\,\boldsymbol{I} \quad (50)$$

while UFZ calculated a swelling stress increment through an additional strain source term as a function of change in saturation:

$$d\boldsymbol{\sigma}^{sw} = \sigma_{max}^{sw}\, dS_w\, \boldsymbol{I} \quad (51)$$

where σ_{max}^{sw} is the maximum swelling stress in the tests.

3 Calibration of the models on laboratory tests

The main objective of the laboratory tests was to characterize the hydro-mechanical response of the bentonite-sand mixture chosen as sealing core material. The available laboratory test results were then used for the calibration of the material models' parameters.

The laboratory tests carried out were the following:
- Water retention tests under both constant volume and free swell conditions;
- Infiltration test under constant volume condition;
- Swelling and compression tests under suction control condition.

These tests, as well as the main characteristics of the bentonite-sand mixture, are described in details in Wang et al. (2013a and 2013b). Hereafter, only the main features of these laboratory tests are recalled.

3.1 Description of the laboratory tests

Materials and samples preparation

The bentonite-sand mixture was made of MX80 bentonite (GELCLAY WH2) and quartz sand (TH1000) in dry weight proportions 70/30. The MX80 bentonite unit mass is 2.77 Mg/m^3, and the sand unit mass is 2.65 Mg/m^3. All the samples were prepared to reach 11% water content by mass. The mixture was then compacted statically to different target dry densities. All the tests were performed in a room with temperature controlled at 20±1°C.

Determination of water retention curves

To investigate the unsaturated hydraulic properties of the bentonite-sand mixture, experiments were performed to determine water retention curves (WRC) under constant volume conditions on samples (50 mm diameter, 5 mm height) placed in a rigid cell. In addition, the water retention curve under free swell conditions was also determined for comparison, but on slightly smaller samples (35 mm diameter and 5 mm height). In both cases (constant volume and free swell), the samples were pre-compacted at a dry density of 1.67 Mg/m^3, corresponding to an initial suction of about 65 MPa.

From an experimental point of view, both the vapour equilibrium technique (high suction range $4.2 < s < 309$ MPa) and the osmotic technique (low suction range $s < 4.2$ MPa) were used to control suction. As shrinkage may occur upon drying, it was not possible to maintain the volume of the sample constant in drying paths. Thus, only wetting paths were followed for the constant volume condition. The results for both conditions are plotted on Figure 1.

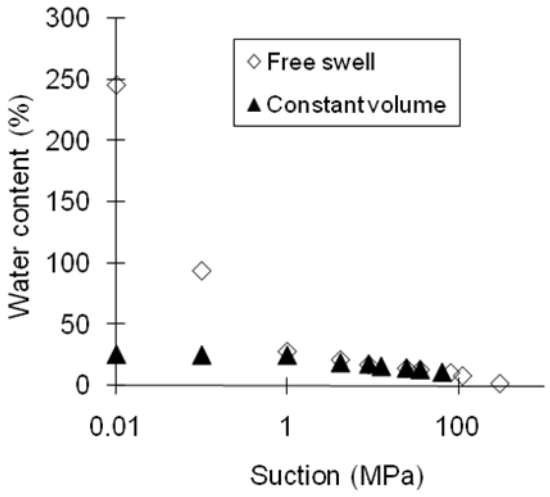

Figure 1 . Data for the water retention curve of bentonite-sand mixture from Wang et al. (2013b)

Infiltration test under constant volume condition

An infiltration test under constant volume condition was carried out in order to investigate the unsaturated hydraulic conductivity of the bentonite-sand mixture at a pre-compacted dry density of 1.67 Mg/m^3. The specimen (50 mm in diameter, 250 mm in height) was put in a metallic cylinder in order to prevent any radial displacement. The two flat ends were covered by metallic discs, the bottom base consisted of water inlets and porous ceramic plate that were used for water supply. Variations of relative humidity (RH) at four distances from the wetted end (h= 50, 100, 150, 200 mm) were monitored during hydration.

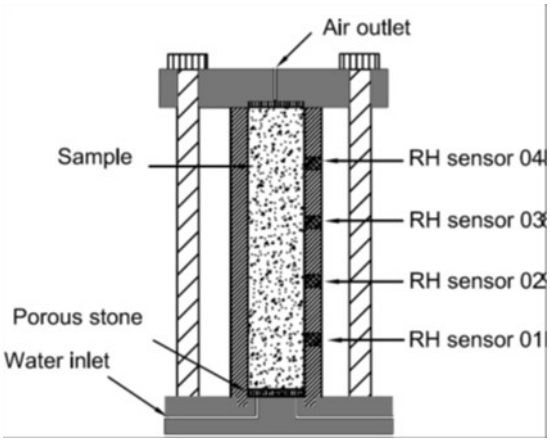

Figure 2. Schematic setup of the infiltration tests under constant volume condition; from Wang et al. (2013a)

The initial relative humidity (RH) was 62±1%, which corresponds to a suction equal to 64.5±1.5 MPa based on the psychometric (Kelvin's) law. The evolution of the relative humidity at different vertical positions versus time is displayed on Figure 3. The suction profiles in the specimen at different times are interpolated accordingly, using Kelvin's law. They are depicted on Figure 4.

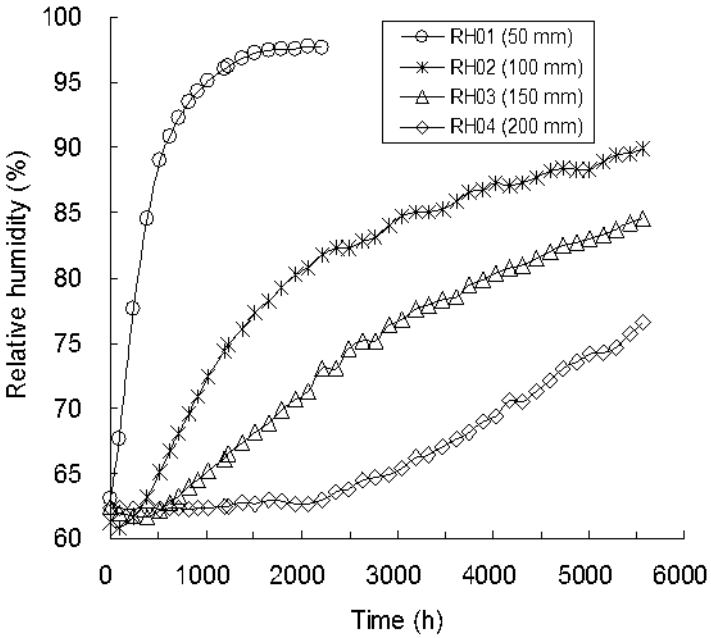

Figure 3. Evolution of relative humidity during infiltration test from Wang et al. (2013a)

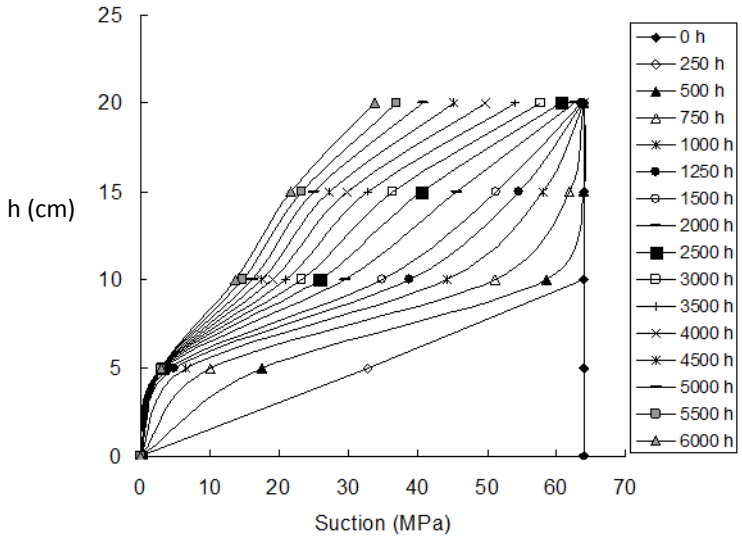

Figure 4. Suction profiles at different times; modified from Wang et al. (2013a)

Swelling and compression tests under suction control condition

The hydro-mechanical behaviour of the bentonite-sand mixture was investigated by means of swelling tests under suction control conditions, followed by compressive tests. Four tests were performed in an oedometric cell, with an internal diameter of 38 mm. In the swelling tests, the axial expansion of the cylindrical samples was free, whereas it was constrained in the radial direction, except for the test SO_01. The test program is summarized in Table 2.

Table 2. Test program

Tests	Initial dry density (Mg/m^3)	Initial diameter (mm)	Applied suction (MPa)
SO-01	1.97	35.13	0.0
SO-02	1.67	38.00	4.2
SO-03	1.67	38.00	12.6
SO-04	1.67	38.00	38.0

All samples had a 10 mm thickness. Test SO-01 differed from the other three tests in that it was conducted on a sample compacted at a dry density of 1.97 Mg/m^3, and with a smaller initial diameter (35.13 mm) in order to leave an initial annular void between the sample and the oedometer. As a consequence, the initial suction in sample SO-01 was a priori different from the other samples (which is about 65 MPa), but it was not measured and had to be derived from the water retention curve for modelling purposes.

Suction imposition was performed under a low vertical pressure of 0.1 MPa. During this process the swelling strain was recorded. After having reached the stabilisation of swelling, compression loading (up to 50 MPa)-unloading cycles were applied to the sample under suction control condition.

a) Behaviour upon suction imposition

The final stabilized axial swelling strain is 1.23%, 5.38%, 6.8% and 18% for a suction of 38 MPa, 12.6 MPa, 4.2 MPa and 0 MPa, respectively (Wang et al., 2013b). For Samples SO-02, -03 and -04, the axial strain is equal to the volumetric strain because there was no radial swelling. Sample SO-01 also swelled radially so the volumetric swelling strain is greater than 18%.The axial swelling strains from the oedometer test are plotted alongside swelling strains from the WRC tests under free swell conditions (Figure 5). These samples were able to swell radially as well as axially, but only the volumetric deformation was measured after suction equilibrium. It can be seen that the swelling strains measured in the WRC tests under free swelling condition are higher than that of the oedometer tests. This is because the WRC samples were able to swell radially whereas 3 oedometer tests had no radial strain and the fourth (SO-01) had up to 8% radial strain.

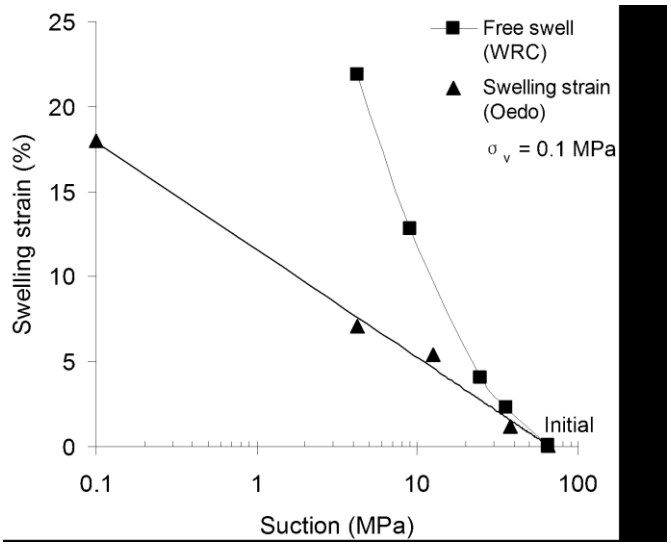

Figure 5. Axial swelling strain versus suction for the free swell oedometer tests and volumetric strain for the WRC tests under free swell condition; modified from Wang et al. (2012)

b) Behaviour upon axial loading-unloading cycle

Figure 6 shows the variation of void ratio with vertical applied stress during the compression process under different constant suction values. The initial points of the loading process are different since they correspond to the final swelling strains induced by the suctions imposed in the previous step. The void ratio *e* has been calculated from the swelling strain using the following expression:

$$e = e_0 + tr(\boldsymbol{\epsilon})(1 + e_0) \quad (52)$$

where e_0 is the initial void ratio, and $tr(\boldsymbol{\epsilon})$ the trace of the strain tensor.

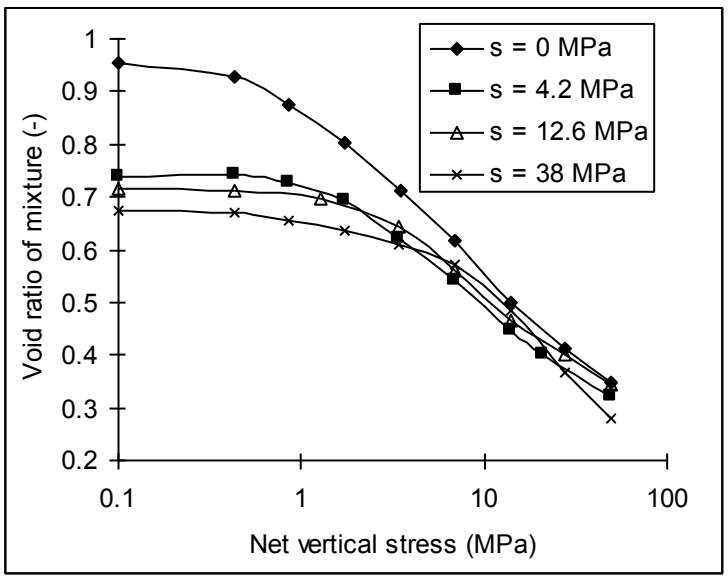

Figure 6. Compression loading-unloading curves following the suction imposition; modified from Wang et al. (2013b)

3.2 Models results

The modelling teams calibrated their constitutive model parameters for the bentonite-sand mixture using the different laboratory tests. Unfortunately, it turned out that the experimental data, which were mostly obtained for a bentonite-sand mixture with an initial dry density of 1.67 Mg/m^3 were not sufficient to obtain a unique calibration of some

models parameters. Thus, the modelling teams revisited completed calibrations from earlier tests during the whole course of the Task, based on the results of other tests. In particular, it was realized that a constant water retention curve was not capable of reproducing the various experiments, and that it should incorporate, in one way or another, the effects of the variations of the material dry density. Here, only the final results obtained by the teams are presented, based on their best calibration of the parameters.

Constant volume water retention curve

Figures 7 and 8 present the water retention curves respectively under constant volume condition and under free swell condition, as obtained from the laboratory tests and as modelled by some of the teams. The other teams did not try to reproduce these experimental results.

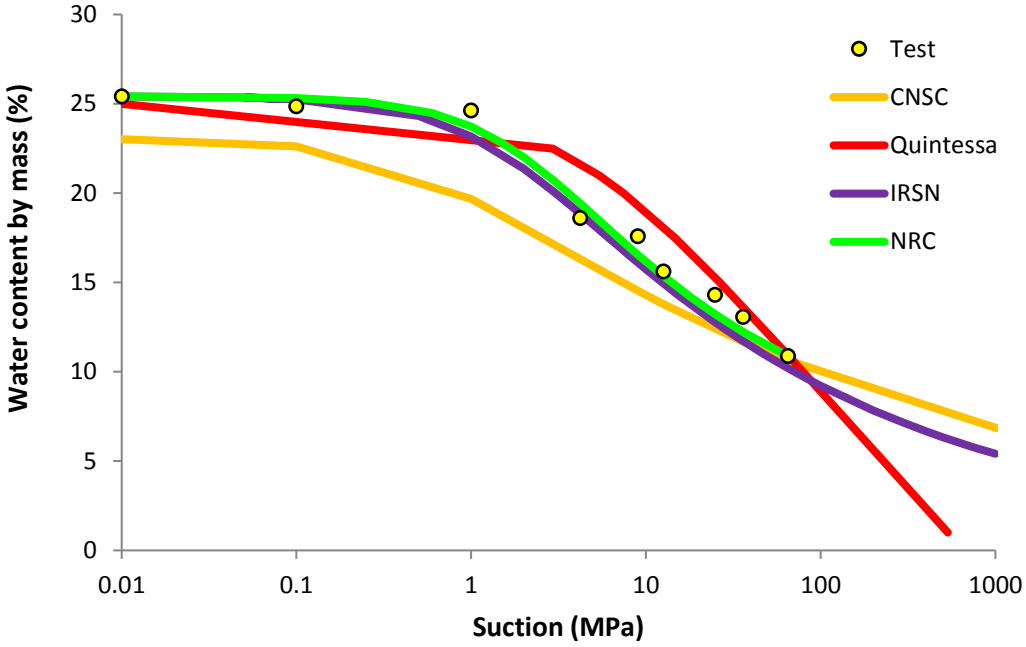

Figure 7. Water retention curve under constant volume condition

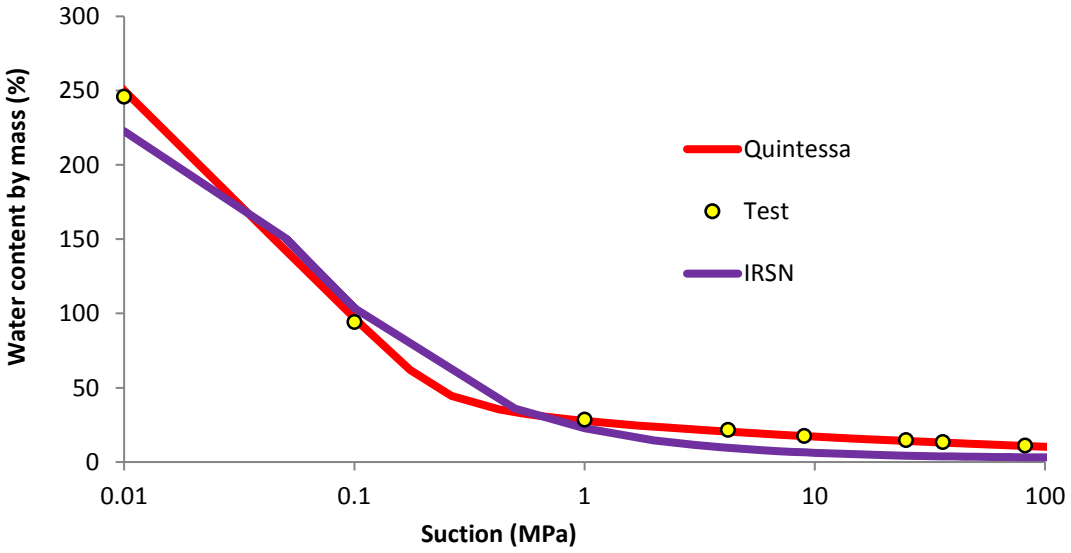

Figure 8. Water retention curve under free swell condition

In the case of constant volume condition, the dry density of the sample remains constant during the test, equal to the initial dry density 1.67 Mg/m^3, whereas in the case of free swell condition, the dry density evolves during the test as a consequence of the continuous change of the volume of the sample. Therefore, the modeling of this second test requires some modifications of the classical water retention curve, as explained above.

Free swelling oedometer tests

The values of the free swelling vertical strain measured in the oedometer for different suction levels and predicted are compared in the table 3.

Table 3. Comparison of measured and predicted free swelling vertical strains

Swelling strain (%)	S=0 MPa	S=4.2 MPa	S=12.6 MPa	S=38 MPa
Test	**18**	**6.8**	**5.38**	**1.23**
IRSN	39.1	4.6	6.0	2.9
NRC	17.4	5.3	2.7	1.55
Quintessa	17.8	6.78	4.41	1.61
UGN	21.1	8.8	5.4	1.8

While there is an overall agreement for the three non-zero suction levels, it can be noticed that the predictions are more scattered for the zero suction level. This is due to the fact that, for this particular case, the bentonite-sand mixture has been compacted to a higher dry density (1.97 Mg/m^3) and the sample had a smaller initial diameter (35.13 mm) in order to leave an initial annular void between the sample and the oedometer. Therefore, the accurate prediction of the free swelling strain is more difficult.

Infiltration test

Figure 9 presents a comparison of the results obtained for the infiltration tests by the different teams.

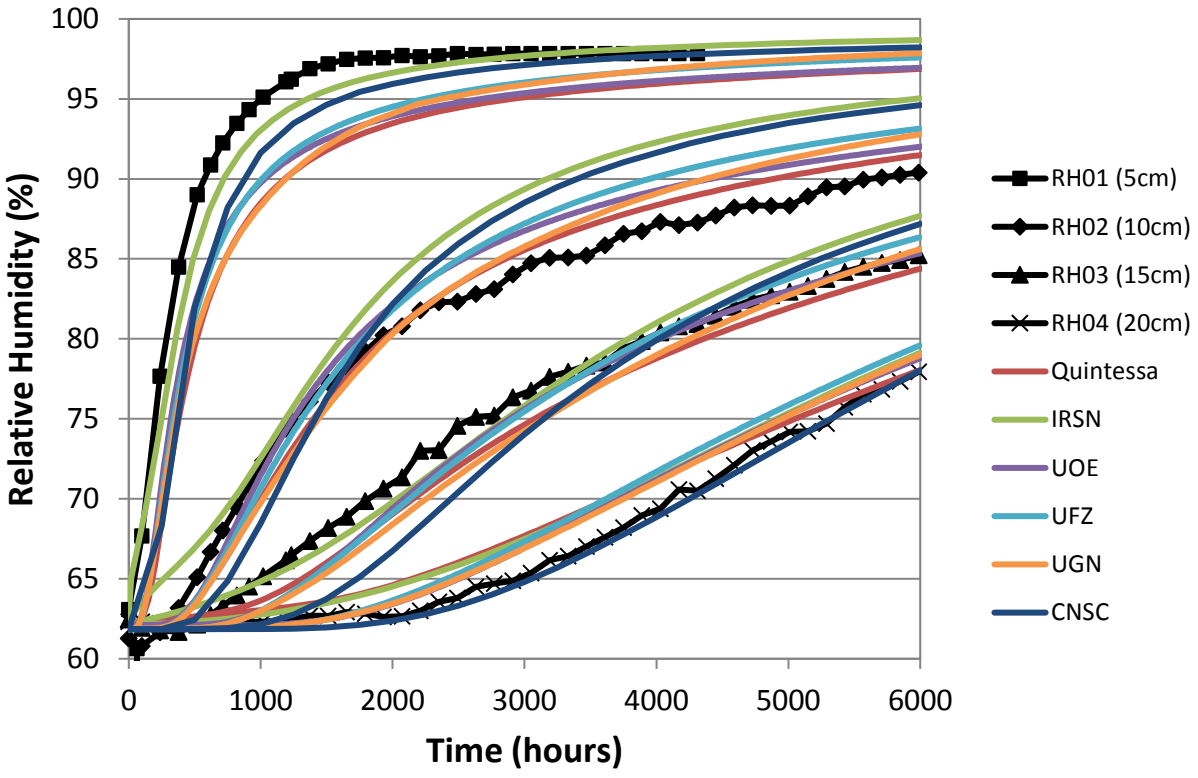

Figure 9. Comparison of RH evolutions and predicted results

The degree of matching between predictions and experimental resultsappears reasonably good. Most of the Teams succeeded in reproducing some of the experimental curves, or some parts of the curves, but did not reach an agreement on all the curves for the whole duration of the experiment.This suggests that hydro-mechanical coupling might not be well represented. Indeed, at the bottom where hydration takes place, the mixture tends to swell, thus leading to an increase in porosity and permeability, while in the upper part of the sample, since the overall volume is constant, the mixture is compressed and its permeability is reduced.

Compression oedometer tests

The experimental results obtained for the compression oedometer tests, for different levels of controlled suction, are compared on Figures 10 to 13 to the predictions by the different teams. The overall trend is satisfactory. The linear dependence of the Young's modulus with regards to the mean pressure, as used by Quintessa, leads to a fair agreement.

Some teams did not model the zero suction compression test. Indeed, this test appears again to be the more difficult data set to model. This is due on one hand to the fact that for very low suctions, the bentonite tends to become a gel, with low mechanical strength, and on the other hand to the fact that this test was performed on a sample with a lower diameter and with a higher initial dry density. Therefore, contrary to the three other tests, the initial state of the sample at the beginning of the compression loading was unknown, and had to be predicted.

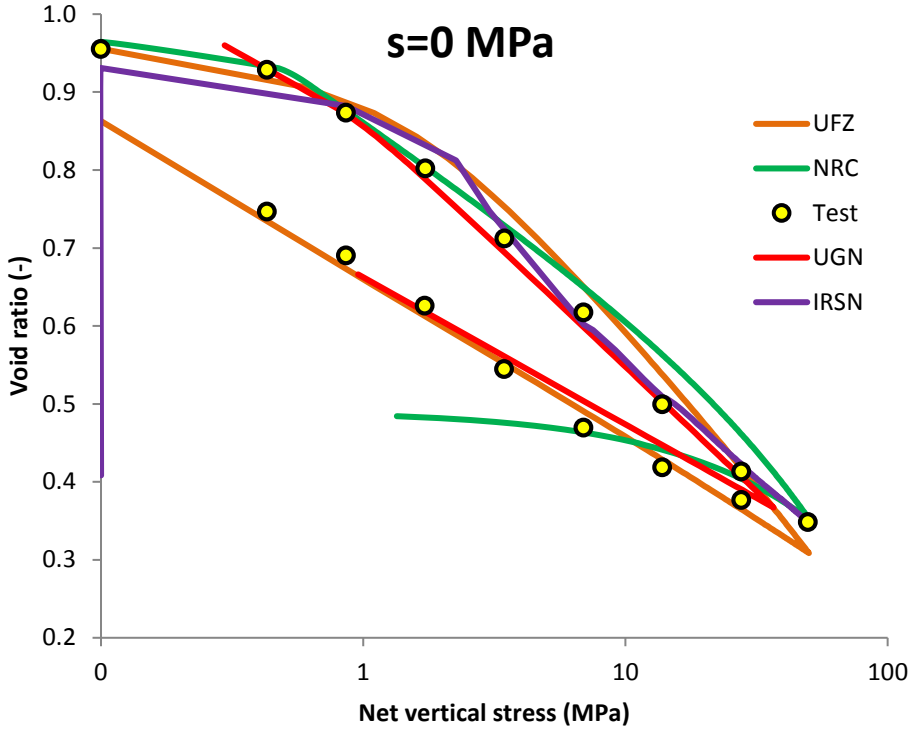

Figure 10. Comparison of compression oedometer test for s=0 Mpa

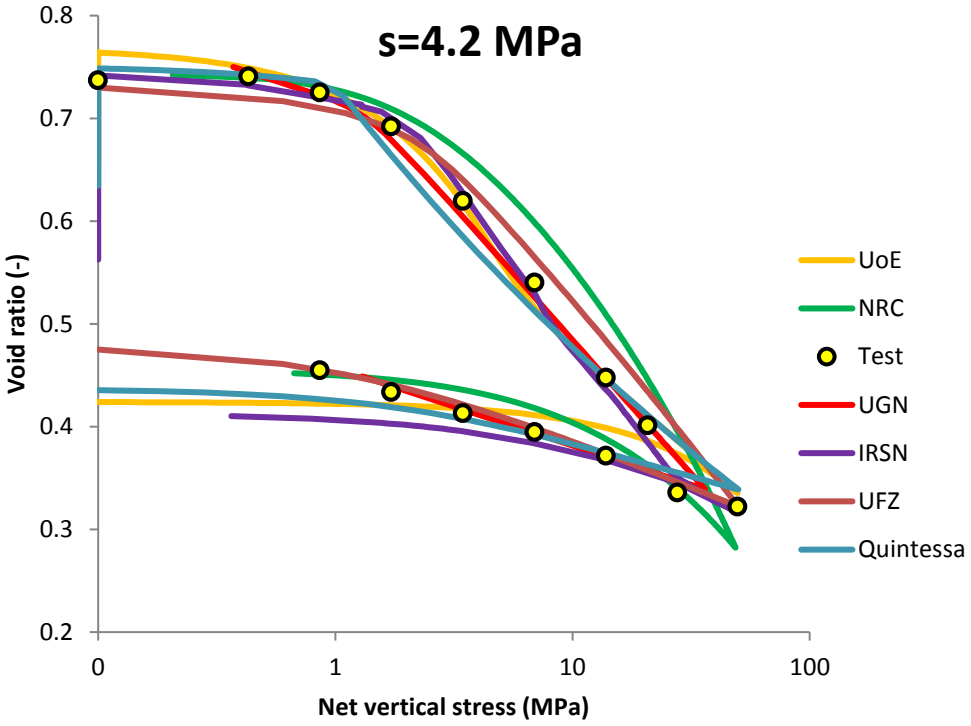

Figure 11. Comparison of compression oedometer test for s=4.2 Mpa

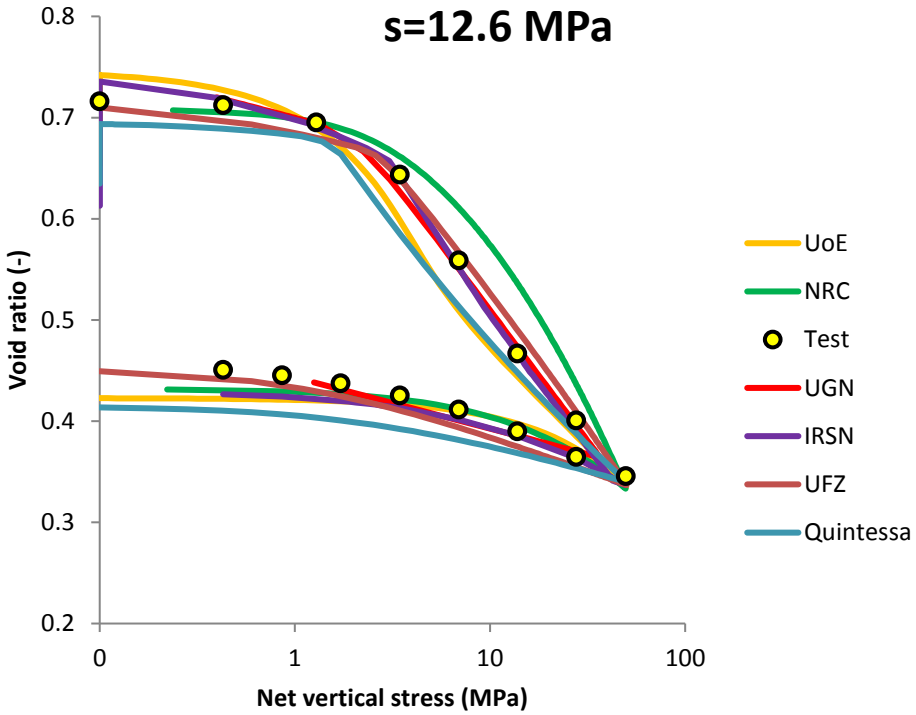

Figure 12. Comparison of compression oedometer test for s=12.6 Mpa

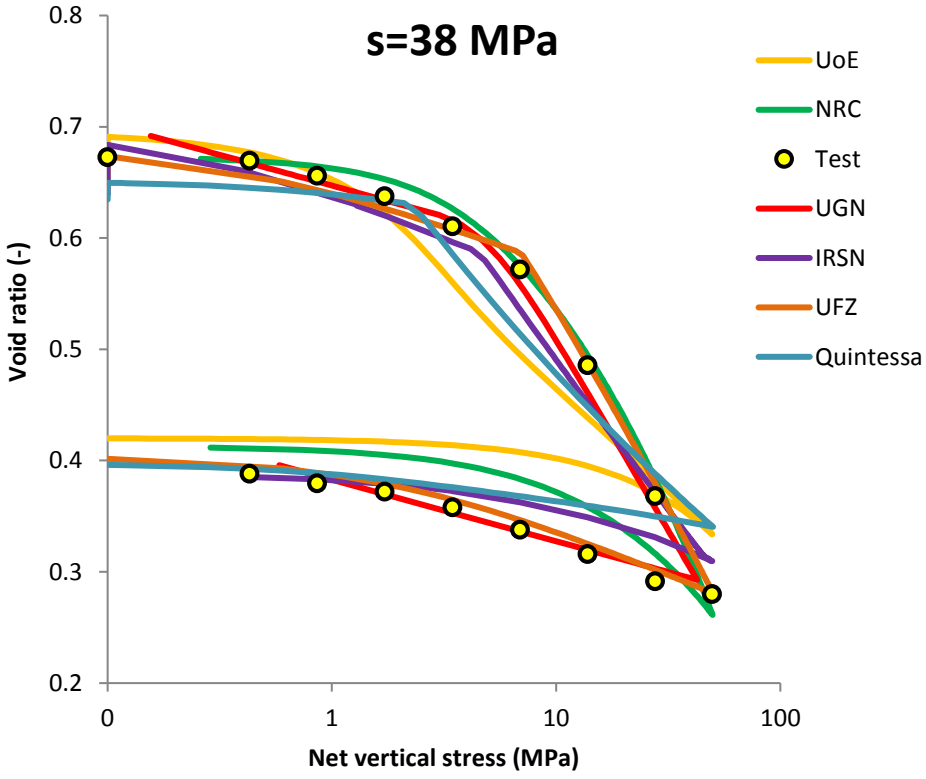

Figure 13. Comparison of compression oedometer test for s=38. MPa

4 Modelling of the mock-up test

The main objectives of this second modelling step were to validate the previously calibrated hydro-mechanical material models by applying them to a 1/10th scale mock-up representative of an in-situ sealing experiment.

4.1 Description of the mock-up test

The 1/10th scale mock-up test aimed to reproduce the behaviour of the bentonite-sand mixture of the SEALEX experiment, but with two major simplifications. Firstly, the rock was replaced by an undeformable steel containment system. Secondly, the mock-up test is vertical, and as such, the annular thickness of the void between the cylindrical sample of bentonite-sand mixture and the container was uniform. For the full-scale in situ tests, the annular void is asymmetrically distributed radially around sealing core that rests on the bottom of a horizontal borehole. Moreover, unlike the mock-up, water can be supplied by the surrounding rock in the radial direction.

In the mock-up test, a compacted sample of bentonite-sand mixture of 120 mm height and 55.5 mm diameter was placed in a rigid (stainless steel) hydration cell of 200 mm length and 60 mm inner diameter. The experimental setup is shown in Figure 14. The cell diameter was greater than the sample diameter to simulate the technological void that exists in the in situ SEALEX experiment, between the bentonite seal and the surrounding rock-mass. The piston was 60 mm in diameter and 150 mm long. The base of the sample was in contact with a porous ceramic disc of 50 mm diameter that contained two water inlets (1 mm in diameter). A mechanical press was used to restrict the vertical displacement and a force transducer was used to monitor the swelling pressure. A Linear Variable Differential Transformer (LVDT) fixed on the piston with an accuracy of 0.001 mm allowed monitoring the swelling strain when needed. The data (axial pressure and displacement) were recorded automatically with a data logger.

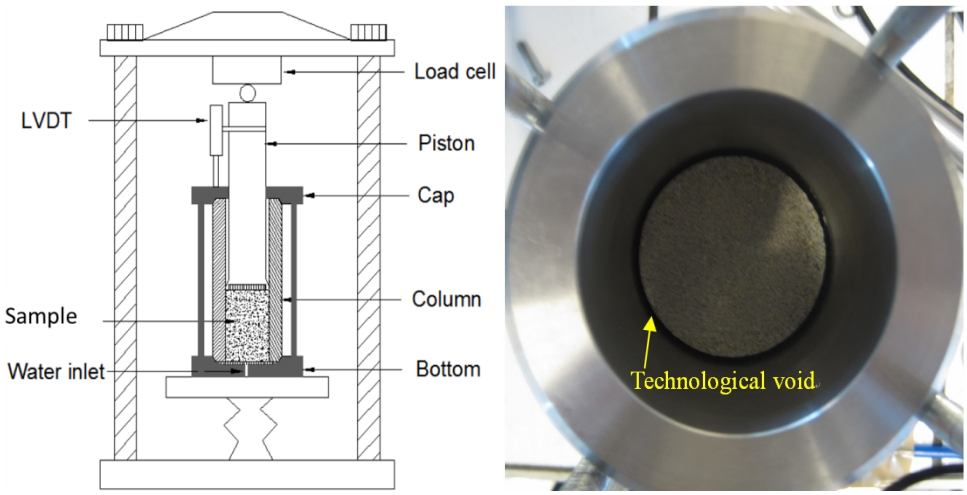

Figure 14. Experimental setup and detail of the technological void between sample and cell

The bentonite-sand mixture specimen was statically compacted in a cylindrical mould to a dry density of 1.97 Mg/m^3. To ensure the homogeneity of the specimen, the compaction was performed in 2 layers. The surface of the compacted first layer was carefully scarified before the next layer was added to ensure a good contact between both. After compaction, the specimen was emplaced in the center of the infiltration cell. While the water inlets of the hydration cell were closed, a 0.07 MPa vertical stress was applied to ensure good contacts between the load cell and the piston, between the piston and the sample, and between the sample and the bottom. After stabilization under the vertical stress, a vacuum was applied and synthetic in situ water was injected from the bottom of the cell at atmospheric pressure

- In the line with the key processes of the sealing systems as described in the introduction, the hydration was performed in three phases (Figure 15) simulating the evolution of the buffer material upon wetting when considering a technological void:

- **Initial saturation** occurred under zero vertical displacement at the top of the sample whilst water was injected into the sample. During this process the evolution of the axial (i.e. vertical) swelling pressure was monitored at the top of the sample. This phase ended once the axial swelling pressure was stabilized;
- **Recovery of void** started when the confining pressure was removed by unloading allowing a free swell of 20%. To reduce the test duration in this stage, two-side infiltration is applied by injecting water from both the bottom and the top while recording changes in axial swelling strain over time;
- **Confinement** occurred by blocking the piston whilst continuing to allow water inflow from the top and bottom of the sample. Axial swelling pressure was recorded during this phase.

Further details on the experiment are reported in Wang et al. (2013b).

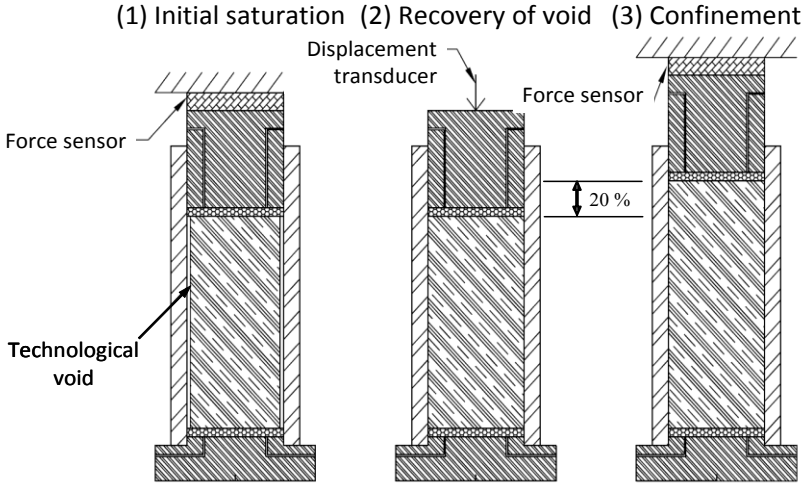

Figure 15. A schematic description of the three phases of the experiment

The objecctive of the modelling was to replicate the measurements (axial pressure and displacement) recorded during the three phases of the experiment. The preliminary phases of equilibrium and vacuum application were not modelled. Instead, it was agreed to start the modelling exercise when hydration started. The corresponding initial stress conditions were a 0.03 MPa compression axial stress and zero radial and orthoradial stresses.

4.2 Modelling of the technological void

The presence of the technological void in the experiment presents additional complexity in how to represent the hydro-mechanical behavior of the void in the model. The process of bentonite/sand mixture swelling to fill technological gaps has been also investigated by Saba (2014). microfocus X-ray tomography (μCT) observations revealed that swelling takes place by clay exfoliation from the bentonite grains around the sample and by creation of a gel. As the void closes, the hydro-mechanical properties of this gel evolve.

Most of the teams used an axisymmetric representation of the mock-up test, but handled the annular void between the sample and the container differently. Experimental evidence indicated that the water immediately flooded the void at the start of the experiment. In order to account for the presence of the technological void, UFZ started with a free radial displacement and a prescribed water pressure at the lateral boundary of the bentonite and then changed to zero radial displacement and zero water flux when the gap was closed. Quintessa modeled this feature by imposing a hydrostatic pressure condition together with an inflow volume limited to the void volume. In addition, they treated the contact between the sample and the container by a specified stress that increased as the sample expanded radially and had a very large value when the sample had filled the void. IRSN used additional finite elements to mesh the void, with particular hydro-mechanical parameters to account for the presence of the water and the possible contact.

In the same spirit, UGN treated the void as a saturated porous material with a very low initial dry density, which gradually increased as the gap closed. The gap is treated as a specific material – a gel like substance with a low elastic modulus and high porosity in the beginning and material close to the standard bentonite-sand mixture in the final stage. The evolution of the gap is a function of the constitutive model, which includes evolution of the elastic modulus, see the expression (44), and evolution of the permeability through Kozeny-Carman relation. The gap is modelled as fully saturated before closing and therefore it serves as a transport zone for the water. CNSC also modelled the technological gap by means of a pervious layer. For the mechanical aspects, the technological void was represented by an elastic spring with spring constant initially very low (0 MPa) that gradually increased to 4 GPa when the maximum displacement of 0.25 mm (thickness of the technological void) was reached. This change in properties of the spring was meant to simulate the initial free swelling of the sample as it expands into the technological void, followed by the restraint of the sample as swelling brings it into contact with the wall of the hydration cell. For the hydraulic aspects, the permeability depended on the gap opening, as part of the constitutive model. The side boundary conditions were changed to no-flow boundaries as the sample swelled and made contact with the wall of the hydration cell. In the UoE model, a moving mesh was used to record when the void becomes filled and to switch on or off the boundary conditions as a function of the nodal displacements. For the hydraulic process the boundary condition was that of water at atmospheric pressure and this remained constant until the nodal radial displacement reached the limit of the technological void space. Once a node was calculated to have reached a displacement equal to the filling of the void, the hydraulic boundary condition was removed. For the mechanical process, the technological void represents a free boundary and as such allows deformation up until the node reaches a displacement equal to the filling of the void. At this point the mechanical boundary becomes a zero displacement boundary. Experimental evidence (Saba 2014) suggests that the technological void was initially filled with a bentonite gel that was not considered in the model. Therefore the technological void likely filled more quickly than predicted by the model. Furthermore, this influences the amount of water that can enter the model through the vertical boundary.

4.3 Model results for the mock-up test

One major difficulty in the modelling was that the initial dry density of the bentonite-sand mixture was 1.97 Mg/m^3, whereas most of the previous calibration tests used a bentonite-sand mixture of 1.67 Mg/m^3 dry density. Insufficient data were available for the high dry density.

*Results of phase 1 (**initial saturation**)*
In this first phase, the vertical deformation was restrained and water was injected to the sample. The evolution of the axial (i.e. vertical) swelling pressure, as measured at the top part of the sample, and predicted by the teams, is compared on Figure 16.

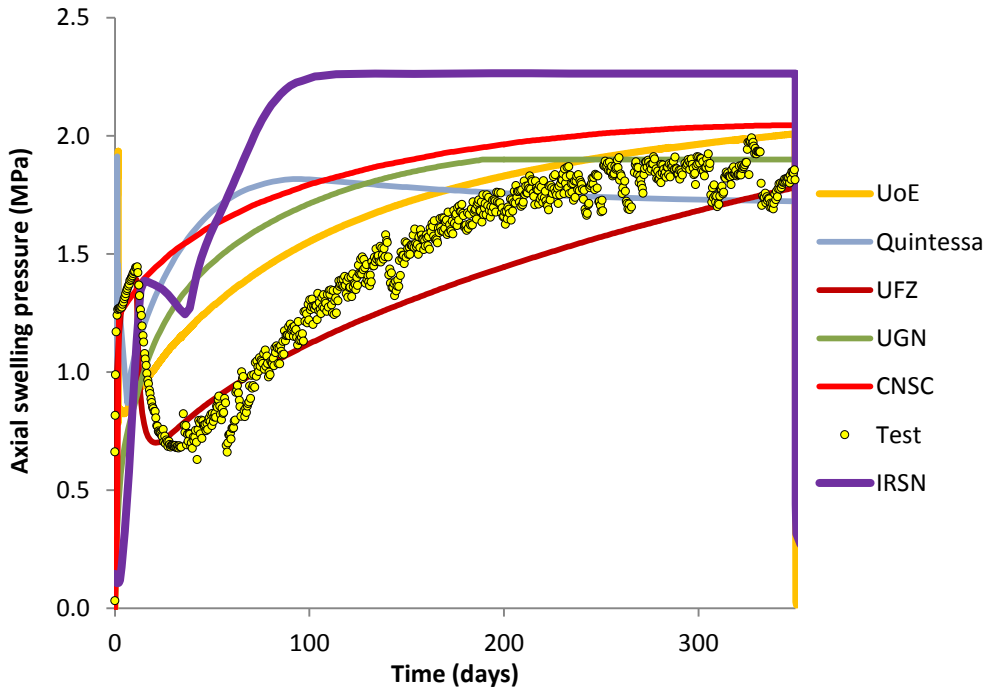

Figure 16. Comparison between measured and predicted swelling pressure

The data show a decrease in swelling pressure at around 20 days which is probably related to the collapse of the bentonite macro-structure. Its modelling requires a plastic component to be included in the mechanical material model. Indeed, this is the case for the IRSN and Quintessa teams, who obtained qualitatively such an instability at the beginning of the response. From the IRSN simulation, it can be observed that important volumetric plastic strains develop during phase 1 (Figure 17), in particular because of the compression induced in the upper part of the sample, and close to the axis, as a reaction to the swelling caused by the hydration on the bottom and side surfaces. However, UFZ was able to reproduce the decrease of the axial pressure using a simple linear elastic material model with a consideration of initial increase pressure by the side surface due to infiltration of water from technological void..

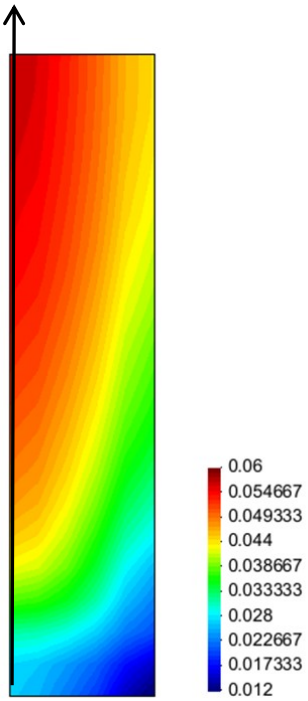

Figure 17. Contours of plastic volumetric deformation (dimension-less) at the end of Phase 1, as calculated by IRSN. Sample axis is on the left, positive strains are contractions.

The injected water volume shows a sharp increase at the start of the experiment (Figure 18) corresponding to the instantaneous flooding of the annular void (Figure 14), which amounts to 49 ml. Then, the volume of injected water increases to a value close to the total volume of void at the beginning of the test, estimated at about 69 ml. Most of the teams reproduce fairly well the experimental measurement (which means that they correctly capture the void ratio variations), while some predictions tend to be slightly over-estimated. There are some differences on the kinetics, which may be attributed to the differences in permeability.

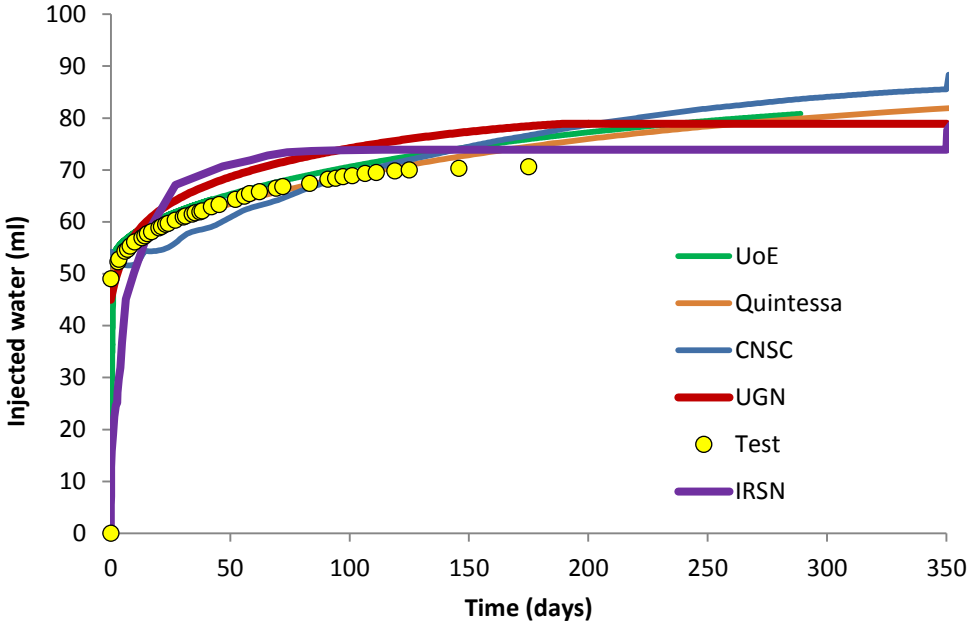

Figure 18. Comparison between measured and predicted injected water volume

*Results of phase 2 (**recovery of vertical void**)*

Phase 2 (labelled 'recovery of vertical void') started once the axial swelling pressure was stabilized. The confining pressure in the axial direction was then removed allowing the vertical free swelling. Changes in vertical strain with time were recorded. In fact, this phase has been divided in two steps : first, water was injected by the bottom face of the sample only, in continuity with phase 1, until the axial strain reached 2.80 %. Then, water was injected by the bottom and top faces of the sample. For the blind prediction of step 1, the time corresponding to this modification of the water injection was supposed to be a result of the modelling, and therefore was not shown. Only Quintessa tried to predict the time at which Phase 2b started, whereas the other teams used as input data the time that was measured during the test.

The predicted axial displacements are compared to the measured one on Figure 19. Compared to the elasto-plastic models, most of the elastic material models tend to over-predict the vertical displacement that occurs instantaneously when the vertical restraint is released. The CNSC team underestimated the value of the vertical displacement upon the removal of the piston. This comes from the use of a linear elastic soft spring to represent the top boundary in order to provide stability to the numerical solution.

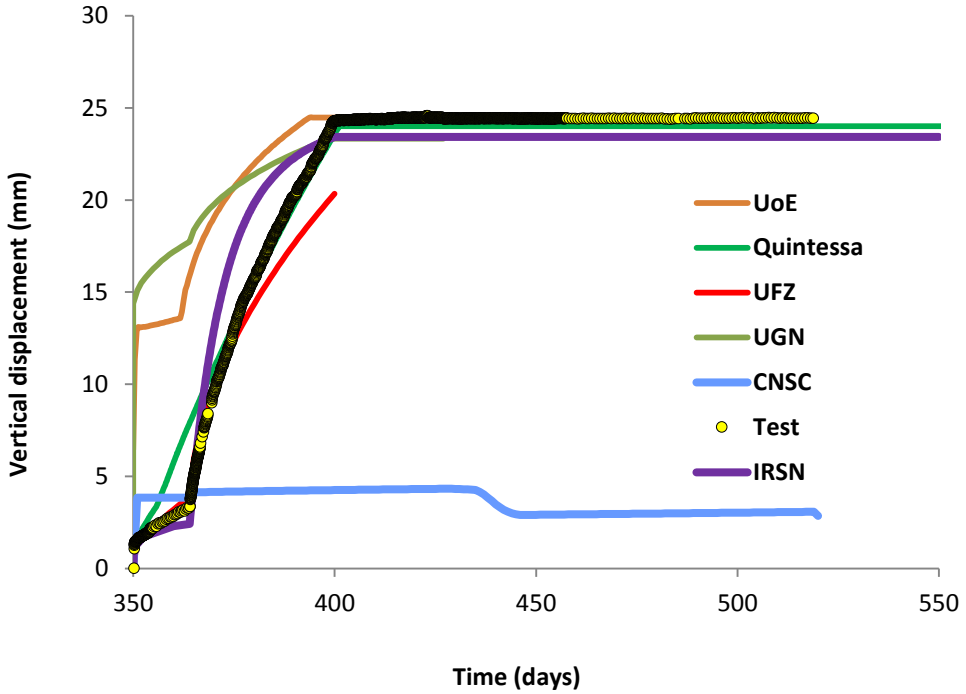

Figure 19. Comparison between measured and predicted vertical displacement

*Results of phase 3 (**confinement**)*

Once the vertical swelling strain reached the maximum value of 20%, the piston was again blocked and the evolution of axial swelling pressure was observed again. During this third and last phase, water injection by the bottom and top faces was maintained. Quintessa and UoE tried to predict the starting time of phase 3, whereas the other teams used the value that was measured during the test. For this reason, the Quintessa and UoE results for phase 3 have been shifted in time for a fair comparison with the other teams. The predicted axial swelling pressures are compared to the measured one on Figure 20.

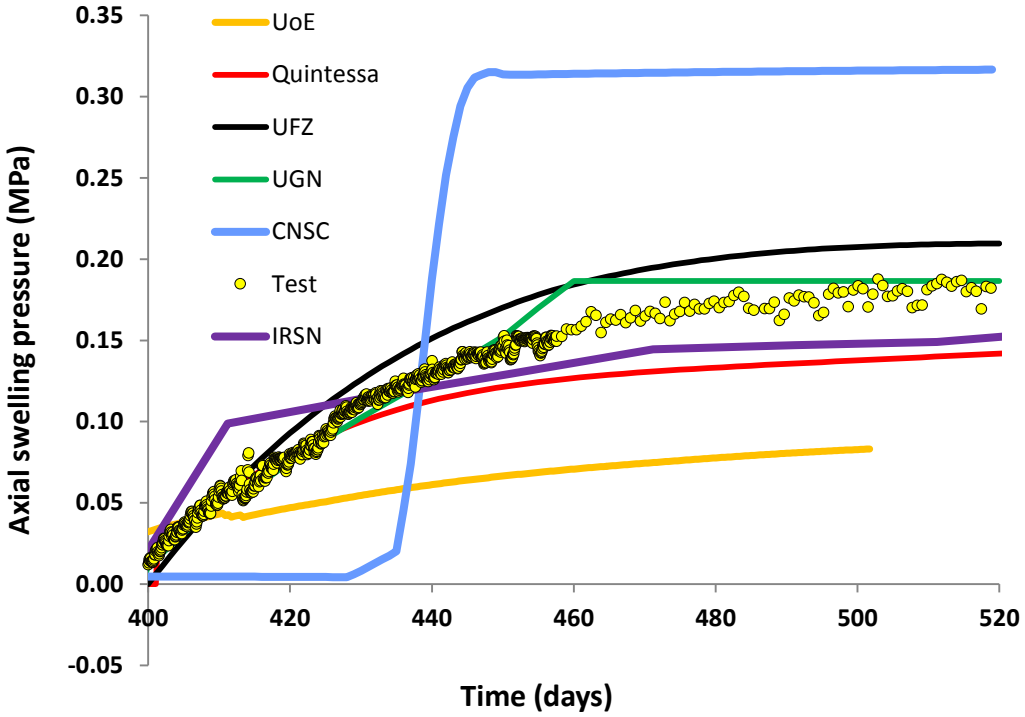

Figure 20. Comparison between measured and predicted swelling pressure

The benchmark modelling of the mock-up test was a challenge for the models of expansive bentonite. The results obtained show that, despite the lack of data for highly compacted bentonite-sand mixture, most of the teams were able to reproduce the main features of the test. However, in general, they had to prescribe the starting times of the different phases rather than to predict them, although a good model should be able to supply this information as well. The unusual axial swelling pressure upon the re-application of the vertical confinement from the CNSC`s simulation is due to the simplified linear elastic model used in the present simulation where the swelling coefficient was assumed to be a function of suction change only, ignoring the effect of stress change induced by the change in the vertical confinement pressure. A revised model using the Basic Barcelona Model (Alonso et al., 1990) was later implemented by the CNSC, and the simulated results compared substantially better with the experimental data (Nasir et al., 2016).

5 Summary of the identified mechanisms/processes

The analysis of the laboratory tests performed in the framework of the SEALEX project included the identification and discussion of possible processes that may influence the test results and more particularly the bentonite-sand behaviour. The modelling work carried out in this project allowed for the assessment of the relevance of a number of processes that must be properly addressed:

- Hydraulic processes in the bentonite-sand mixture can be represented by Richard's equation (or full multi-phase flow), provided that vapour diffusion is taken into account;
- The change of permeability with dry density and saturation is important and models have been able to match major trends, but details (such as in the infiltration test) are still difficult to capture;
- An accurate representation of the retention curve is necessary, and in particular, its dependence on the dry density (or porosity) of the bentonite. In addition, including a representation of the double porosity character of this material in the suction curve improved results. A single water retention test under constant volume is not sufficient to characterize the retention curve, and a water retention test under free swelling is preferred.
- For the mechanical aspects, the bentonite-sand mixture clearly shows an elasto-plastic response under certain stress-suction paths. Although many teams obtained satisfactory results in the simulation of the mock-up test while using an elastic (non-linear) behaviour, a realistic predictive material modelling should incorporate such features.
- Because of the large swelling capacity of the bentonite, an additional swelling strain has to be incorporated in many classical constitutive models.

- The dry density of the bentonite-sand mixture and its evolution with time has a crucial influence on the hydro-mechanical behaviour of the material. As a consequence, a full characterization of the material requires performing laboratory tests at different dry densities.
- The presence of the technological void adds considerable complexity to the load-suction path. The core is first subjected to a constrained swelling under hydration in the axial direction, but to a free swelling in the radial direction. Then, when the gap is closed, the swelling occurs under constrained volume in both directions, but with a reduced hydration from the lateral side. A good representation of the void is crucial to getting sensible results.

6 Conclusions

The laboratory tests performed as part of the SEALEX experimental program have formed the basis for a successful and fruitful task consisting of modelling a $1/10^{th}$ scale mock-up of the sealing system. Through modelling the range of laboratory tests, a major challenge was finding a unique set of parameters able to correctly simulate all the experiments. Some teams identified a unique set of parameter values; others relied on different parameters calibrated for each experiment. This challenge is due to the fact that the bentonite properties strongly depend on its dry density, which varies as saturation and mechanical stress vary. Another point for improvement concerns the modelling of the technological void, which exists initially between the bentonite-sand core and the oedometer wall. It was realized during the task that its hydro-mechanical behaviour is important, evolving from the state of a gel when hydration starts, towards the state of compacted bentonite when the gap is closed. Altogether, the task has enabled a better understanding of the complex hydro-mechanical behaviour of the bentonite-sand mixture, and consequently an improved modelling of this material. The overall good agreement between the tests results and the computer simulations constitutes a validation of the numerical tools that have been developed during the task. In addition, the task has demonstrated the important role of the technological void on the short-term behaviour of the sealing system. With regards to this particular point, an accurate modeling of this phase will require additional research on the exfoliation of the core under hydration at its outer boundaries, which creates a bentonite-based gel and on its progressive hardening under compaction. The consistent results between the different codes and the measurements are an important validation of the numerical tools.

Acknowledgement

The work described in this paper was conducted within the context of the international DECOVALEX Project. The authors are grateful to the Funding Organisations who supported the work. The views expressed in the paper are, however, those of the authors and are not necessarily those of the Funding Organisations. Nor do the views expressed herein necessarily reflect the views or regulatory positions of the U.S. Nuclear Regulatory Commission (USNRC), and do not constitute a final judgment or determination of the matters addressed or of the acceptability of any licensing action that may be under consideration at the USNRC.

References

Alonso, E. E., Gens, A., Josa, A. 1990 A constitutive model for partially saturated soils. Géotechnique, 40(3) pp. 405-430

Barnichon J.D., Deleruyelle F. 2009 Sealing experiments at the Tournemire URL: the SEALEX Project. Eurosafe

Barnichon J.D., Dick P., Bauer C. 2012 The SEALEX in situ experiments: Performance tests of repository seals. In: Harmonising Rock Engineering and the Environment – Qian & Zhou (eds) © 2012 Taylor & Francis Group, London, ISBN 978-0-415-80444-8, pp. 1391-1394

Baumgartner P. 2006. Generic thermal-mechanical-hydraulic (THM) data for sealing materials. Volume 1: Soil – Water Relationships. Report No: 06819-REP-01300-10122-R00. Atomic Energy of Canada Limited.

Bond AE., Benbow SJ. 2009 QPAC Multi-Phase Flow Module Functional Specification and Architectural Design. Quintessa Report QRS-QPAC-HYD-2 v1.0

COMSOL 2012 COMSOL Multiphysics version 3.5 User's Guide
Dixon D.A., Priyanto D.G., Martino J.B., De Combarieu M., Johansson R., Korkeakoski P., Villagran J. 2014 Enhances Sealing Project (ESP): evolution of a full-sized bentonite and concrete shaft seal. Geological Society, London, Special Publications, 400, doi:10.1144/

Dueck A. 2004 Hydro-mechanical properties of a water unsaturated sodium bentonite, Laboratory study and theoretical interpretation, Doctoral thesis ISBN 91-973723-6-6

Fredlund, D.G., Rahardjo. H. 1993 Soil Mechanics for Unsaturated Soils. John Wiley & Sons, Inc., New York City, New York

Hansen J., Holt E., Palmu M. 2103 Full-Scale Demonstration of Plugs and Seals Euradwaste'13 8th EC Conference on the Management of Radioactive Waste, Community Policy and Research on Disposal, Vilnius, Lithuania

Huertas, F., Fuentes-Santillana, J.L., Jullien, F., Rivas, P., Linares, J., Fariña, P., Ghoreychi, M., Jockwer, N., Kickmaier, W., Martínez, M.A., Samper, J., Alonso, E., Elorza, F.J. 2000 Full-scale engineered barriers experiment for a deep geological repository for high-level radioactive waste in crystalline host rock. EC Final REPORT EUR 19147

Itasca Consulting Group. 2011 *FLAC V 7.0, Fast Lagrangian Analysis of Continua, User's Guide*. Minneapolis, Minnesota, Itasca Consulting Group

Kolditz, O., Bauer, S., Bilke, L., Böttcher, N., Delfs, J. O., Fischer, T., Park, C. H. 2012 OpenGeoSys: an open-source initiative for numerical simulation of thermo-hydro-mechanical/chemical (THM/C) processes in porous media. Environmental Earth Sciences, 67(2) pp. 589-599

Liu L., Neretneiks I., Moreno L. 2011. Permeability and expansibility of natural bentonite MX-80 in distilled water. Physics and Chemistry of the Earth. 36. pp1783-1791

Man, A., Martino J.B. 2009 Thermal, Hydraulic and Mechanical Properties of Sealing Materials. NWMO TR-2009-20. Toronto, Canada: Nuclear Waste Management Organization

Martino,J.B., Dixon D., Stroes-Gascoyne S.,Guo R., Kozak E.T., Gascoyne M., Fujita T., Vignal B., Sugita Y., Masumoto K., Saskura T., Bourbon X., Gingras-Genois 1., Collins D. 2008 The Tunnel Sealing Experiment: 10 Year Summary. Atomic Energy of Canada Ltd., URL-12150-REPT-001, Chalk River

Maul P. 2013 QPAC: Quintessa's general-purpose modelling software. Quintessa report QRS-QPAC-11. www.quintessa.org

Millard A., Mokni N., Barnichon J.D., Thatcher K.E., Bond A.E., Fraser-Harris A., Mc Dermott C., Blaheta R., Michalec Z., Hasal M., Nguyen T.S., Nasir O., Yi H., Kolditz O. 2016 Comparative modelling approaches of hydro-mechanical processes in sealing experiments at the Tournemire URL, Environmental Earth Sciences, submitted

Nasir, O., Nguyen, T.S., Barnichon, J.D., Millard, A. 2016. Simulation of the hydro-mechanical behaviour of bentonite seals for the containment of radioactive wastes. Canadian Geotechnical Journal, submitted

Navarro V., Asensio L., Yustres A., Pintado X. 2015. Characterisation of the volumetric behaviour of MX-80 aggregates using water retention data. Abstract. Clays in Natural and Engineered barriers for Radioactive Waste Confinement, Brussels

Olivella S., Carrera J., Gens A., Alonso E.E. 1994 Non isothermal multiphase flow of brine and gas through saline media. Transport Porous Media, 15 pp. 271-293

Olivella S., Gens A., Carrera J., Alonso E.E. 1995 Numerical formulation for a simulator (CODE_BRIGHT) for the coupled analysis of saline media. Engineering Computations, 13 pp. 87–112

Quintessa. 2013 QPAC: Quintessa's General-Purpose Modelling Software QRS-QPAC-11. http://www.quintessa.org/qpac-overview-report.pdf

Richards L.A. 1931 Capillary conduction of liquids through porous mediums. Journal of Applied Physics, 1 (5) pp. 318–333

Saba S. 2014 Comportement hydromécanique différé des barrières ouvragées argileuses gonflantes, PhD Thesis, Université Paris Est, France (in French)

Thatcher K.E., Bond A.E., Robinson P., McDermott C., Fraser Harris A.P., Norris S. 2016 A new hydro-mechanical model for bentonite resaturation applied to the SEALEX experiments, Environmental Earth Sciences, DOI: 10.1007/s12665-016-5741-z

van Geet M., Bastiaens W., Volckaert G., Weetjens E., Sillen X., Gens A.,Villar M.V., Imbert C., Filippi M., Plas F. 2007 Installation and evaluation of a large-scale in-situ shaft seal experimet in Boom clay – The RESEAL project. International conference on clays in natural and engineered barriers for radioactive waste confinement, Lille, France

van Genuchten, M.Th. 1980 A closed-form equation for predicting the hydraulic conductivity of unsaturated soils. Soil Science Society of America, 44(5) pp. 892-898

Villar M.V., Campos R., Gutiérrez-Nebot L. 2014 EB experiment Laboratory post-mortem analyses report CIEMAT Technical Report CIEMAT/DMA/2G210/01/2014

Wang Q., Tang A.M., Cui Y.J., Delage P., Gatmiri B. 2012 Experimental study on the swelling behaviour of bentonite/claystone mixture. Engineering Geology, 124 pp. 59-66

Wang Q., Tang A.M., Cui Y.J., Barnichon J.D., Saba S., Ye W.M. 2013a Hydraulic conductivity and microstructure changes of compacted bentonite-sand mixture during hydration Engineering Geology, 164 pp. 67-76

Wang Q., Tang A.M., Cui Y.J., Delage P., Barnichon J.D., Ye W.M. 2013b The effects of technological voids on the hydro-mechanical behaviour of compacted bentonite-sand mixture Soils and Foundations, 53(2) pp. 232-245